Longitudinal Resistive Wall Wakefields

for the

ILC Positron Undulator Vessel

DUNCAN SCOTT

MAGNETICS & RADIATION SOURCES GROUP:

DARESBURY LABORATORY

ABSTRACT

The DC, AC and anomalous skin effect longitudinal resistive wall wakefields of a round vessel have been computed for the ILC positron source undulator vessel. They have been calculated as a function of vessel radius for copper, aluminium, gold, iron and stainless steel materials and for the minimum, nominal and maximum ILC parameters. Gaussian, trapezium and 'Linac Coherent Light Source type' charge distributions have been modelled as examples. To assess the effects of cryogenic temperatures (the undulator is a superconducting helical device) the wakes have been calculated at 273K and 77K. For an undulator aperture of 5.6mm the increase in energy spread is 2% for gold at 273K with a Gaussian bunch profile and the minimum ILC parameters. The induced energy spread decreases with temperature and at 77K is 1.3% for gold and a Gaussian bunch.

1. Introduction

In the baseline design the positrons for the ILC are produced via pair production in a metallic target using a photon drive beam. The photons are produced using a helical undulator and the main ILC electron beam at 150GeV. For a polarised positron beam there needs to be approximately 200m of active undulator. The helical undulator is a super-conducting bi-filar helix design that has a circular vessel. To create the necessary on axis magnetic field in the helical undulator the aperture of the magnet will be less than 10mm in diameter. As the main electron beam is passing through such a long narrow gap vessel the wakefield effects of the vessel need to be assessed. A general introduction to resistive wall wakefields has already been given [1] and can be found elsewhere [2, 3] in this note the longitudinal wakefield effects are discussed. These change the energy of the beam and induce and energy spread within a bunch. In the minimal set of ILC parameters there is ~150ns between bunches and so only short range wakefields are considered. Resistive wall wakefields of a cylindrical pipe with finite conductivity have been calculated for various bunch charge distributions, vessel materials, vessel radius and the different ILC beam parameter sets. Relevant parameters for the beam and undulator are given in Table 1. The minimum vessel radius is ~2mm, but the current nominal vessel radius is ~2.8mm. Wakes have been calculated up to a 5mm radius.

Parameter	Symbol	Unit	Value		
ILC Mode			Min	Nominal	Max
Rms Bunch Length	σ_z	10^{-6} m	150	300	500
Number of electrons	N	10^{10}	1	2	2
Beam Energy	E	GeV	150		
Nominal RMS Energy Spread	σ_E/E	%	0.05		
Vessel Length	L	m	200		
Vessel radius (min)		mm	2		
Vessel radius (nominal)		mm	2.8		

Table 1: undulator vessel and ILC beam parameters.

2. Conductivity and Impedance Models

In the Drude-Sommerfield model of electron conductivity [4] conduction electrons are treated as an ideal gas obeying Maxwell-Boltzmann or Fermi-Dirac statistics respectively. The conductivity is related to the mean free time between collisions (or metal relaxation time), τ, of the conduction electrons moving in an applied field, or equivalently the mean free path between collisions, l, where:

$$l = v_F \tau ,$$

and v_F is the Fermi velocity for the particular metal.

If the field the electrons are moving in is constant during this time then the conductivity effects are said to be DC. The DC conductivity of a metal, σ_{DC}, is given by:

$$\sigma_{DC} = \frac{ne^2\tau}{m_e},$$

where n is the density of conduction electrons, e their charge and m_e the electron mass. In general the wakefields/impedances can be defined in terms of a characteristic distance, s_0, which is a function of the pipe radius, b, it's DC conductivity, the speed of light, c, and the permittivity of free space, ε_0:

$$s_0 = \left(\frac{2cb^2\varepsilon_0}{\sigma_{DC}}\right)^{\frac{1}{3}}.$$

For a round metallic pipe the DC monopole longitudinal impedance, $Z^0_{\|,DC}$, is:

$$Z^0_{\|,DC}(k) = \frac{Z_0 s_0}{2\pi b^2}\left[\frac{1 - i\,sign(ks_0)}{|ks_0|^{1/2}} + \frac{iks_0}{2}\right]^{-1},$$

where $Z_0 = (c\varepsilon_0)^{-1}$ is the vacuum impedance. As the undulator is super-conducting the wakefield effects at two temperatures, 273K and 77K have been looked at for a variety of different materials. Below 77K values for the conductivity depend upon many factors such as the purity of the material and grain size. Table 2 gives values for σ_{DC} and τ for copper, aluminium, gold and iron [4]. The vessel could be made out of aluminium or stainless steel and then perhaps coated in a thin layer of gold or copper if necessary. Iron has been looked at as values for stainless steel are difficult to obtain. (In section 8 an estimation of the values for stainless steel type 316L has been made.)

	273K		77K	
	σ_{DC}	τ	σ_{DC}	τ
Unit	$(10^7)\Omega^{-1}m^{-1}$	$(10^{-14})s$	$(10^8)\Omega^{-1}m^{-1}$	$(10^{-14})s$
Copper	5.88	2.7	5.00	21
Aluminium	3.62	0.8	3.33	6.5
Gold	5.93	3.0	2.00	20
Iron	1.10	0.23	1.51	3.2

Table 2: DC conductivities and mean time between collisions for different materials at 273K and 77K.

The DC conductivity model assumes that the applied field is constant between electron collisions. If the applied field changes significantly between the collisions then the conductivity is said to be AC and is given by [4]:

$$\sigma_{AC} = \frac{\sigma_{DC}}{1 - i\omega\tau},$$

where ω is the angular frequency of the field. For short bunches the oscillation frequency of the fields from the beam can be shorter than the mean free time between collisions and so both effects need to be calculated. For AC conductivity a dimensionless metal relaxation time, Γ, can be defined which indicates the strength of the AC effects [5]:

$$\Gamma = \frac{\tau c}{s_0},$$

Table 3 gives vales of Γ for a 2mm radius vessel and the various materials considered. From the values of Γ it should be expected that the AC effects at 77K are will be more significant than at 273K for all materials.

	Γ, 273K	Γ, 77K
Copper	1.13	18.0
Aluminium	0.27	4.88
Gold	1.267	12.67
Iron	0.055	1.84

Table 3: values for the dimensionless metal relaxation time at 273K and 77K for a 2mm radius vessel of different materials.

The monopole AC conductivity impedance, $Z^0_{\|,AC}$, can be given in terms of Γ and s_0 [5]:

$$Z^0_{\|,AC}(k) = \frac{Z_0 s_0}{2\pi b^2}\left[\sqrt{\frac{t_\lambda}{\Gamma k^2}}\left(i\sqrt{1+t_\lambda} + sgn(k)\sqrt{1-t_\lambda}\right) - \frac{ik}{2}\right]^{-1},$$

where $t_\lambda = \frac{|ks_0|\Gamma}{\sqrt{1+(ks_0\Gamma)^2}}$.

Another effect that needs to be included is the anomalous skin effect (ASE). If the frequency of the field is not too high then the field will penetrate into a metal a distance δ_0 (the "classical" skin depth) given by [6]:

$$\delta_0(k) = \sqrt{\frac{2}{Z_0\sigma_{DC}k}}.$$

The derivation of the skin depth of a material assumes that the field in the metal varies little over a mean free path, $\delta_0 >> l$. When this assumption is not valid and $\delta_0 \sim l$ the theory of the ASE must be used. For cases where $\delta_0 << l$ the simple picture of an exponentially decaying field breaks down completely and is known as the extreme anomalous regime.

In the Reuter and Sondheimer model of the ASE [7] the ASE surface impedance, Z_{ASE}, is expressed in terms of a ratio to the classical impedance, Z_{cl}. The surface resistive and reactive parts of the impedance ***in CGS units*** are:

$$\frac{R_{ASE}}{R_{cl}}(k) = \frac{\left(4\sqrt{2\alpha(k)}\right)\left(kc\tau\,\mathrm{Re}\left[I(k)\right] - \mathrm{Im}\left[I(k)\right]\right)}{\pi\sqrt{3}\left(1+(kc\tau)^2\right)\sqrt{-kc\tau+\sqrt{1+(kc\tau)^2}}},$$

$$\frac{X_{ASE}}{X_{cl}}(k) = \frac{\left(4\sqrt{2\alpha(k)}\right)\left(\mathrm{Re}\left[I(k)\right] + kc\tau\,\mathrm{Im}\left[I(k)\right]\right)}{\pi\sqrt{3}\left(1+(kc\tau)^2\right)\sqrt{kc\tau+\sqrt{1+(kc\tau)^2}}},$$

where,

$$\alpha(k) = \frac{3}{2}\left(\frac{l}{\delta_0(k)}\right)^2,$$

$$I(k) = \int_0^\infty \left(t^2 + \frac{2i\alpha(k)\left[\left(1+t^2\right)Tan^{-1}(t) - t\right]}{(1+kc\tau)^3 t^3}\right)^{-1} dt\,.$$

The classical expressions for the surface resistance and reactance are:

$$R_{cl} = \sqrt{\frac{2\pi k}{c\sigma_c}}\sqrt{-kc\tau+\sqrt{1+(kc\tau)^2}}\,,$$

$$X_{cl} = \sqrt{\frac{2\pi k}{c\sigma_c}}\sqrt{kc\tau+\sqrt{1+(kc\tau)^2}}\,.$$

Figure 1 and Figure 2 show how the ASE changes the surface impedance for copper at particular frequencies, the resistive and reactive parts can decrease as well as increase. It can also be seen that the effects at lower temperatures are more important, this is to be expected as the mean free path at lower temperatures is greater.

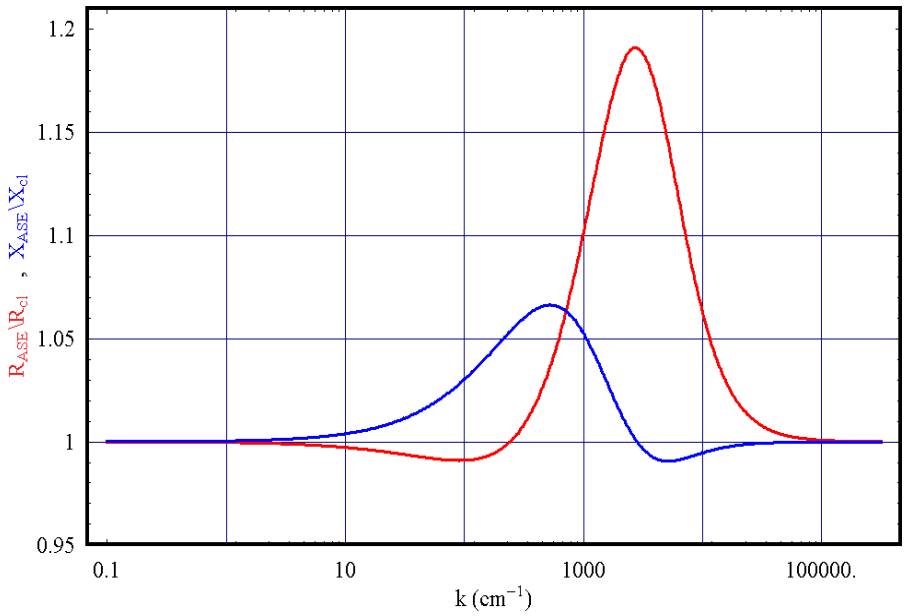

Figure 1: ratio of the ASE to classical surface resistance (red) and reactance (blue) for copper at 273K as a function of the wavenumber of the applied field.

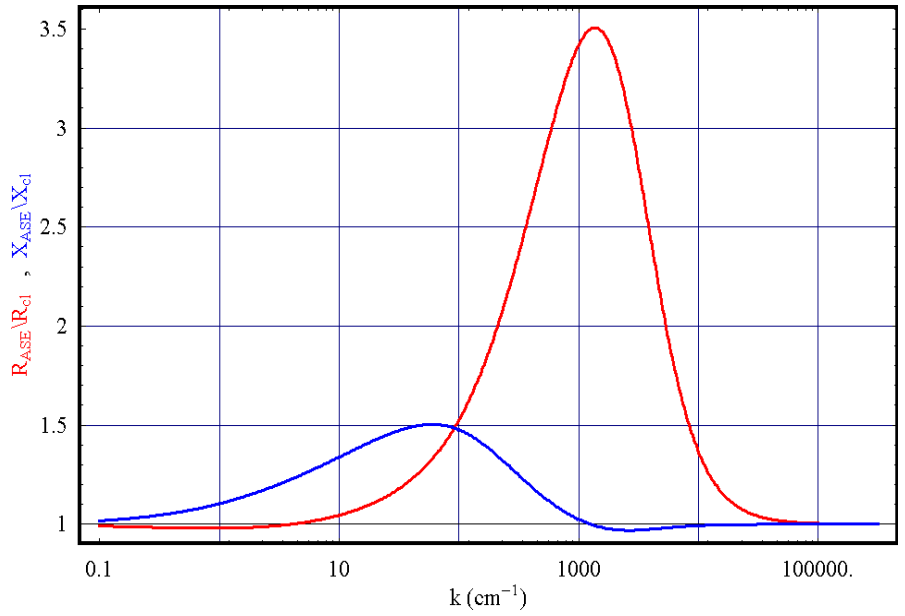

Figure 2: ratio of the ASE to classical resistance (red) and reactance (blue) for copper at 77K as a function of the wavenumber of the applied field.

A dimensionless ASE strength parameter, Λ, can be defined that is also independent of frequency [5]:

$$\Lambda = \frac{\alpha(k)}{kc\tau}.$$

Table 4 gives vales of Λ for the various materials considered at 77K and 273K. From the values of Λ it is expected that the ASE will be more significant at lower temperatures.

	Λ, 273K	Λ, 77K
Copper	3.69	244
Aluminium	1.12	84
Gold	3.27	73
Iron	0.09	17.9

Table 4: values for the ASE strength parameter for different materials at different temperatures.

The monopole ASE longitudinal impedance, $Z^0_{\|,ASE}$, ***in CGS units*** is:

$$Z^0_{\|,ASE}(k) = \frac{1}{\mathrm{bc}}\left(\frac{8\pi|k|}{ck(R_{ASE}[k]Sign[k] - iX_{ASE}[k]} - ibk\right)^{-1}$$

The impedances for the different models are plotted for copper at 273K and 77K in Figure 3 and Figure 4. The resonant peaks for the AC and ASE impedance are much narrower than for the DC impedance. The AC and ASE effects are also more pronounced at 77K, as expected. The imaginary parts of the impedances are odd functions of k and the real parts are even functions of k.

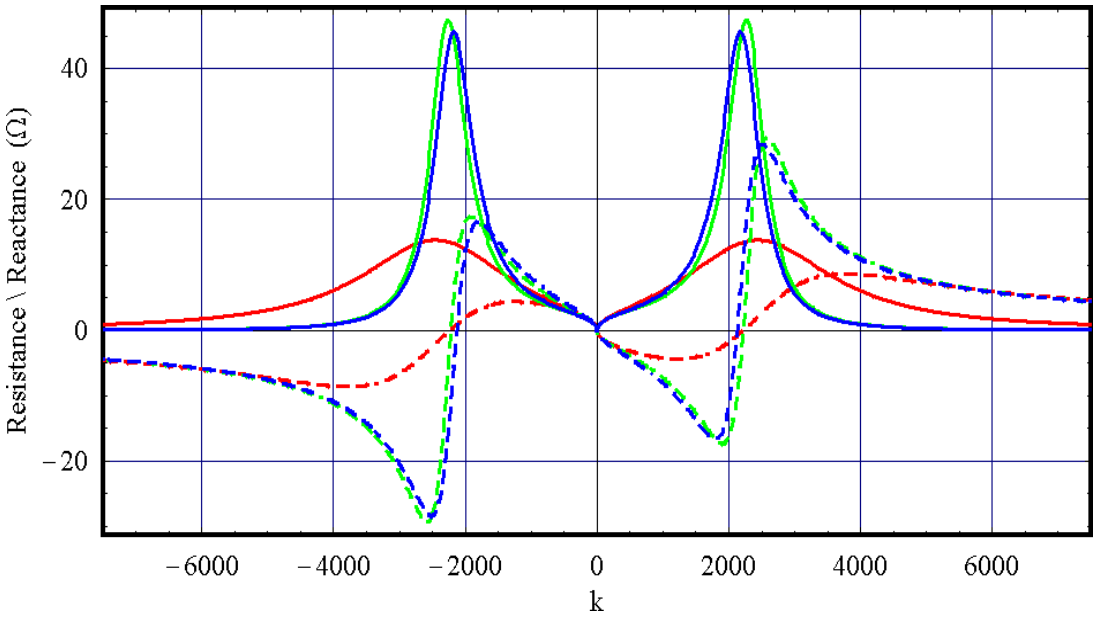

Figure 3: the real (solid) and imaginary (dashed) parts of the impedance for DC conductivity (red) AC conductivity (green) and the ASE (blue) v k, for copper at 273K.

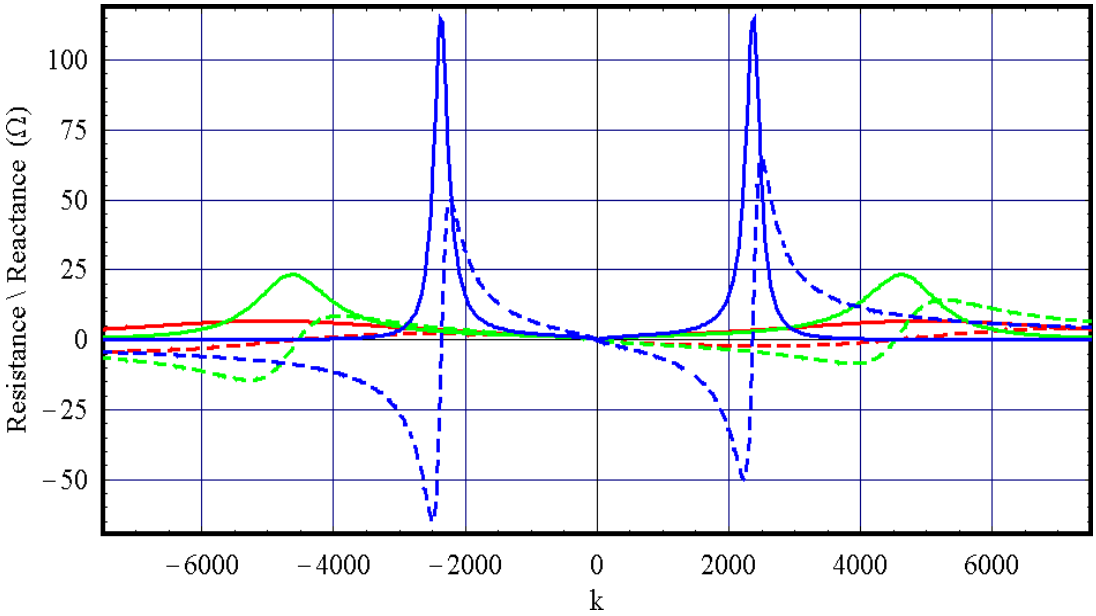

Figure 4: the real (solid) and imaginary (dashed) parts of the impedance for DC conductivity (red) AC conductivity (green) and the ASE (blue) v k, for copper at 77K.

3. Wake Functions

By definition the longitudinal wake function, $w_{\parallel}$, is simply the Fourier transform of the longitudinal impedance:

$$w_{\parallel}(t) = \frac{1}{2\pi}\int_{-\infty}^{\infty} d\omega Z_{\parallel}(\omega) e^{i\omega t}.$$

For the DC conductivity this has been found analytically by substituting $Z^0_{\parallel,DC}(k)$ into $w_{\square,dc}(s) = \frac{c}{2\pi}\int_{-\infty}^{\infty} Z^0_{\parallel,DC}(k) e^{-ikt} dk$ and performing the integration in the complex plane. The result is [8]:

$$w_{\parallel,DC}(s) = -\frac{4}{\pi\varepsilon_0 b^2}\left\{\frac{1}{3}e^{-\frac{s}{s_0}} Cos\left(\sqrt{3}\frac{s}{s_0}\right) - \frac{\sqrt{2}}{\pi}\int_0^{\infty}\frac{x^2}{x^6+8} e^{-x^2\frac{s}{s_0}} dx\right\}.$$

For the AC and ASE impedances the wake function can be found numerically. The Fourier transform can be simplified to,

$$w_{\square}(s) = \frac{2c}{\pi}\int_0^{\infty} \mathrm{Re}\left[Z^0_{\parallel}(k)\right] Cos(ks)\, dk,$$

as only the real part of the impedance has a non-zero value when integrated from minus infinity to plus infinity. The wake function can be thought of as the wake left behind a delta function charge distribution. Figure 5 shows the wake in a copper vessel at 273K and Figure 6 for copper at 77K. At 273K the AC and ASE wakes are

similar and at 77K they are quite different, as expected. The charge is at $s = 0$ and is travelling from right to left.

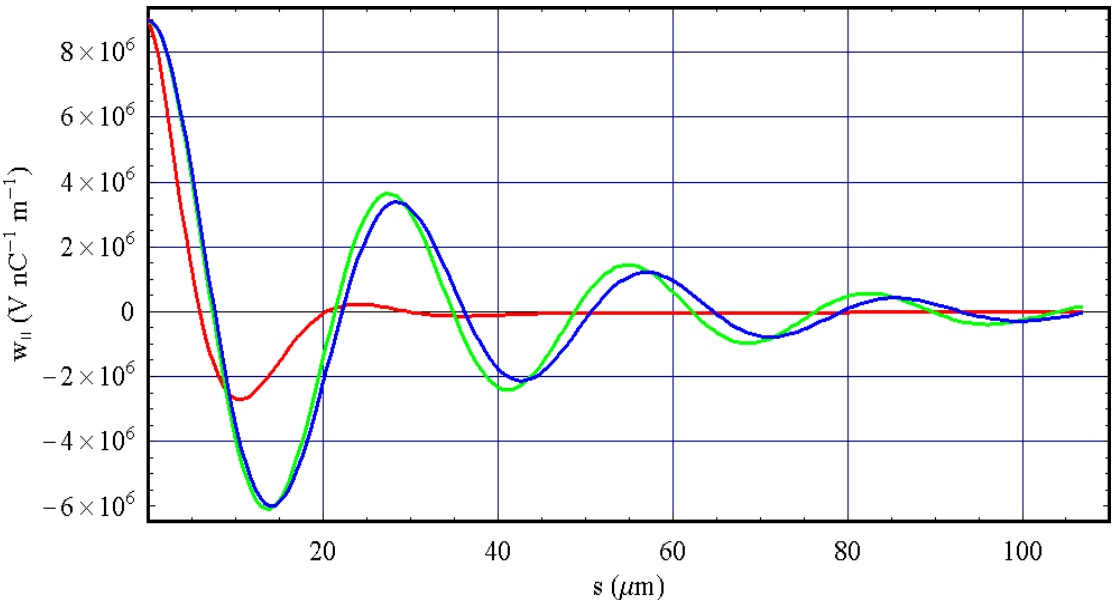

Figure 5: DC conductivity (red) AC conductivity (green) and ASE (blue) wake potentials for a 2mm copper vessel at 273K,

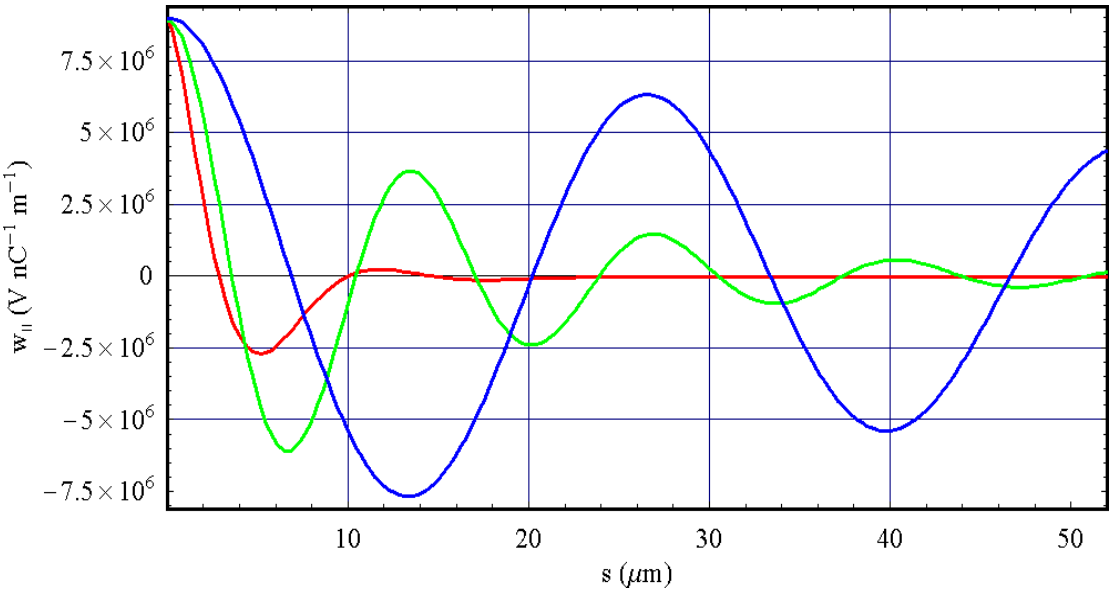

Figure 6: DC conductivity (red) AC conductivity (green) and ASE (blue) wake potentials for a 2mm copper vessel at 273K,

4. Wake Potentials

The longitudinal wake potentials, $W_{\square}$, are found by convoluting the longitudinal wake function with a charge distribution, $\rho(s)$,

$$W_{\square}(s) = \int_{-\infty}^{\infty} \rho(s') w_{\square}(s-s') ds' ,$$

and ρ is normalised such that $\int_{-\infty}^{\infty} \rho(z) dz = 1$. Continuing the example of a copper vessel at 273K and 77K the wake potentials for a Gaussian bunch with $\sigma_z = 150 \mu m$ is shown in Figure 7 and Figure 8. The difference between the AC and ASE wakes again becomes more prominent at 77K. The value of the wakes are much less at 77K, Table 5 gives the values at the centre of the charge distribution, $s = 0$.

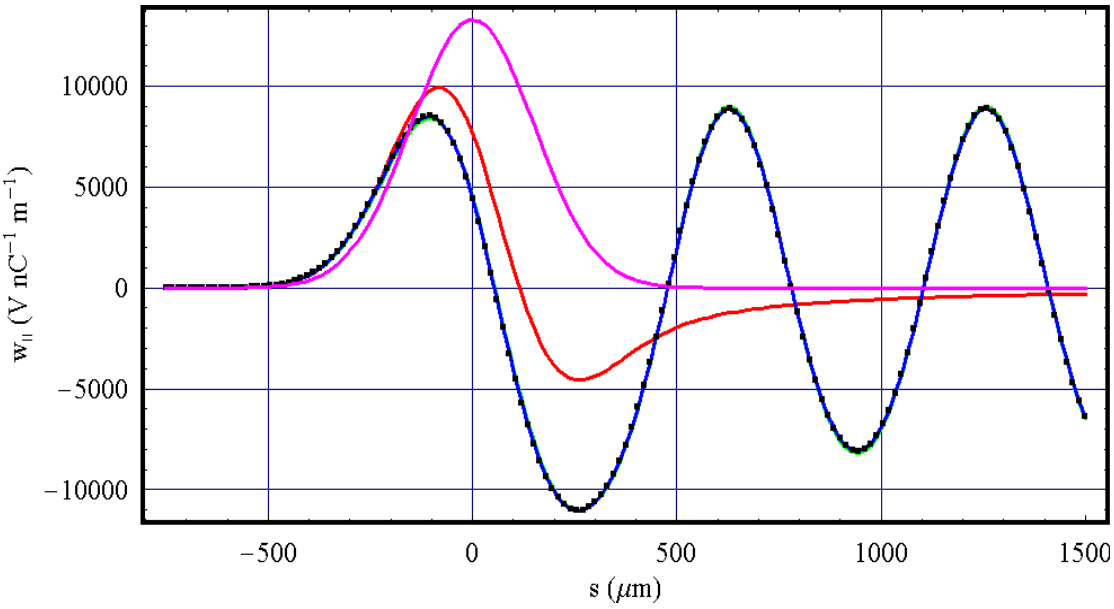

Figure 7: DC (red), AC (green & points) and ASE (blue) wake potentials for a Gaussian charge distribution $\sigma_z = 150 \mu m$ (magenta) and a 2mm copper vessel at 273K.

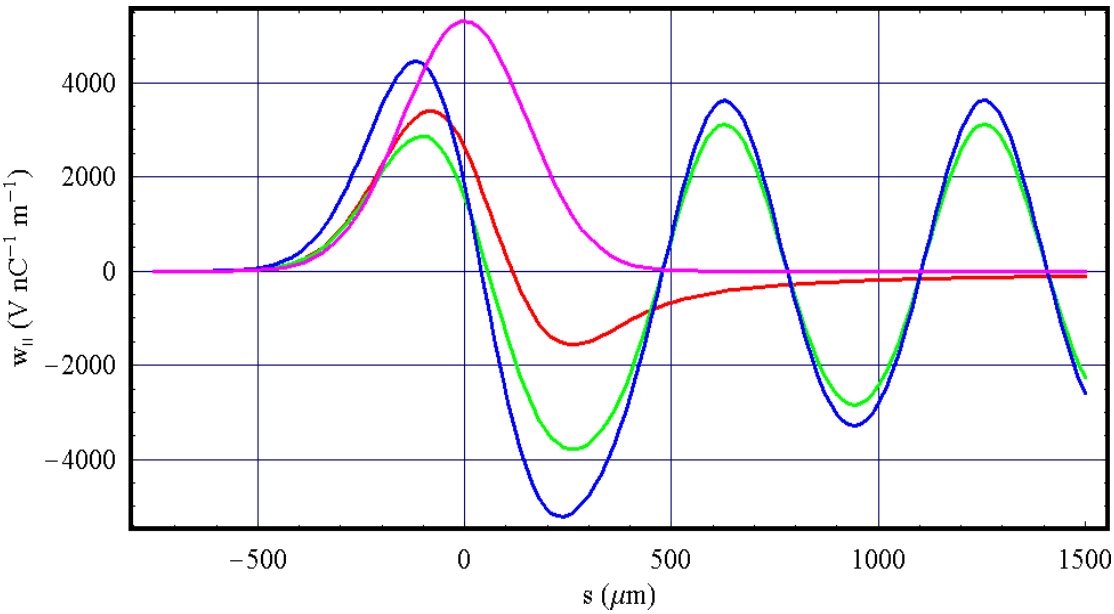

Figure 8: DC (red), AC (green) and ASE (blue) wake potentials for a Gaussian charge distribution $\sigma_z = 150\mu m$ (magenta) and a 2mm copper vessel at 77K.

	Unit	273K	77K
DC Wake	V nC^{-1} m^{-1}	7666	2618
AC Wake	V nC^{-1} m^{-1}	4502	1562
ASE Wake	V nC^{-1} m^{-1}	4442	1811

Table 5: values of the wake potential at $s = 0$ for a 2mm copper vessel and a Gaussian bunch with $\sigma_z = 150\mu m$

6. Energy Lost and Induced Energy Spread

The longitudinal loss factor per meter is given by:

$$k_{\square} = -\int_{-\infty}^{\infty} \rho(s) W_{\square}(s)\, ds\,,$$

from which the induced rms energy spread of the bunch per meter, σ_E, can be calculated:

$$\sigma_E = eN \left| \int_{-\infty}^{\infty} \left(\rho(s) W_{||}^2(s) - k_{\square}^2 \right) ds \right|^{1/2},$$

where N is the number of particles of charge e. The energy lost by the bunch, ΔE, is the work done by the longitudinal electromagnetic force along the structure. This is related to the loss factor by the relation:

$$\Delta E = e^2 N k_{\square}\,.$$

The average energy lost by the bunch is of the order of a few MeV for the worst possible case. **Figure 9** shows the energy lost by a bunch along the entire length of undulator for an iron vessel at 273K. The DC wakes effect dominates and there is little difference between the AC and ASE wakes. From now on the average energy lost from the bunch will not be considered as it is so small.

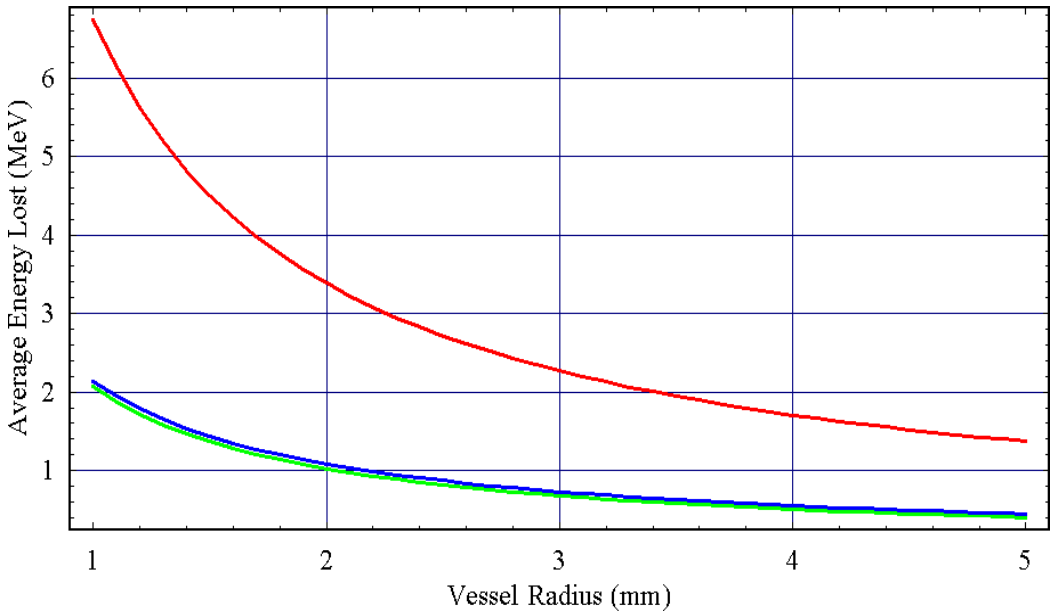

Figure 9: average energy lost by a 150 micron Gaussian bunch for an Iron vessel at 273K from DC (red) AC (green) and ASE (blue) wakes.

The induced energy spread has been calculated for all possible combinations of the values from Table 1 and Table 2 as a function of the vessel radius. Figure 10 shows the induced energy spread for a 150 micron Gaussian bunch, Figure 11 for a 300 micron Gaussian bunch and Figure 12 for a 500micron Gaussian bunch. as the bunch length is increased the wakefield effects are reduced and so only the short, 150 micron bunches will be considered from now on. Similar graphs for aluminium, gold and iron with a 150micron bunch length are shown in Figure 13, Figure 14 and Figure 15.

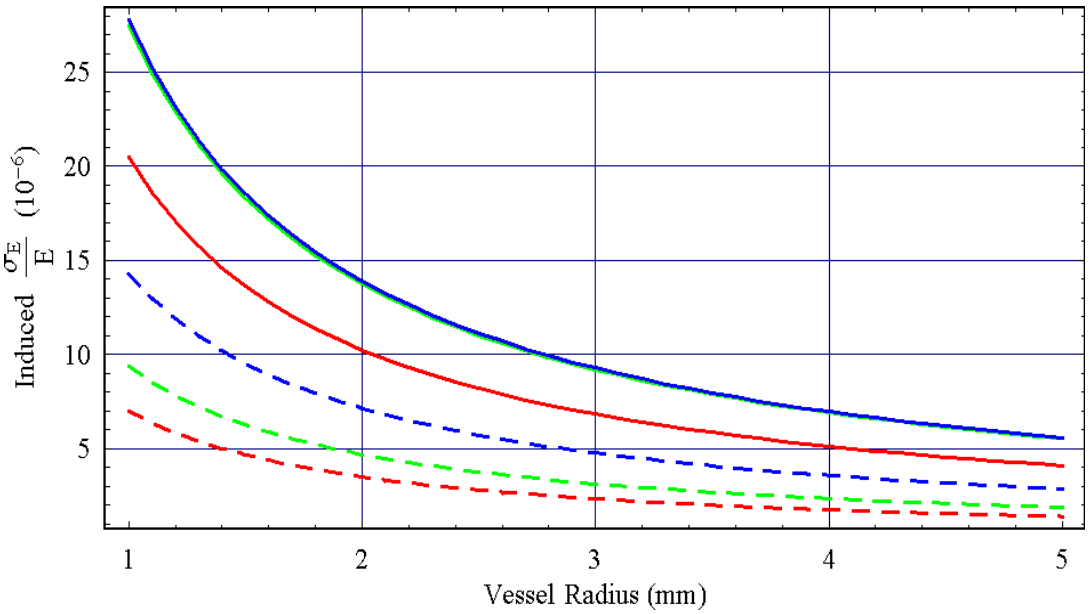

Figure 10: induced energy spread for 200m of undulator for DC (red) AC (blue) and ASE (green) wakes as a function of vessel radius for copper at 273K (solid) and 77K (dashed) for a 150 micron Gaussian bunch.

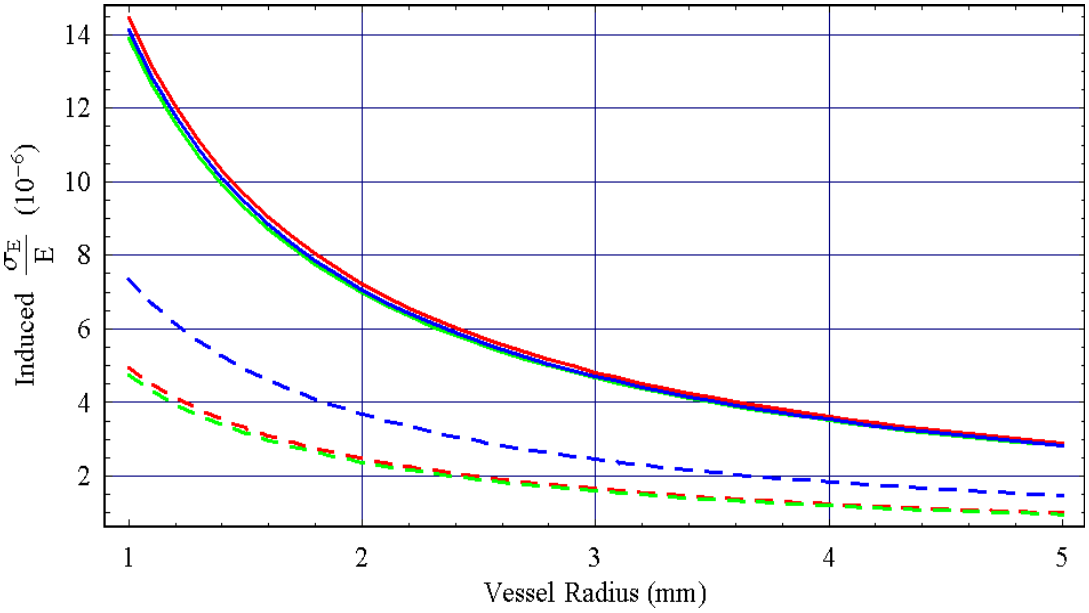

Figure 11: induced energy spread for 200m of undulator for DC (red) AC (blue) and ASE (green) wakes as a function of vessel radius for copper at 273K (solid) and 77K (dashed) for a 300 micron Gaussian bunch.

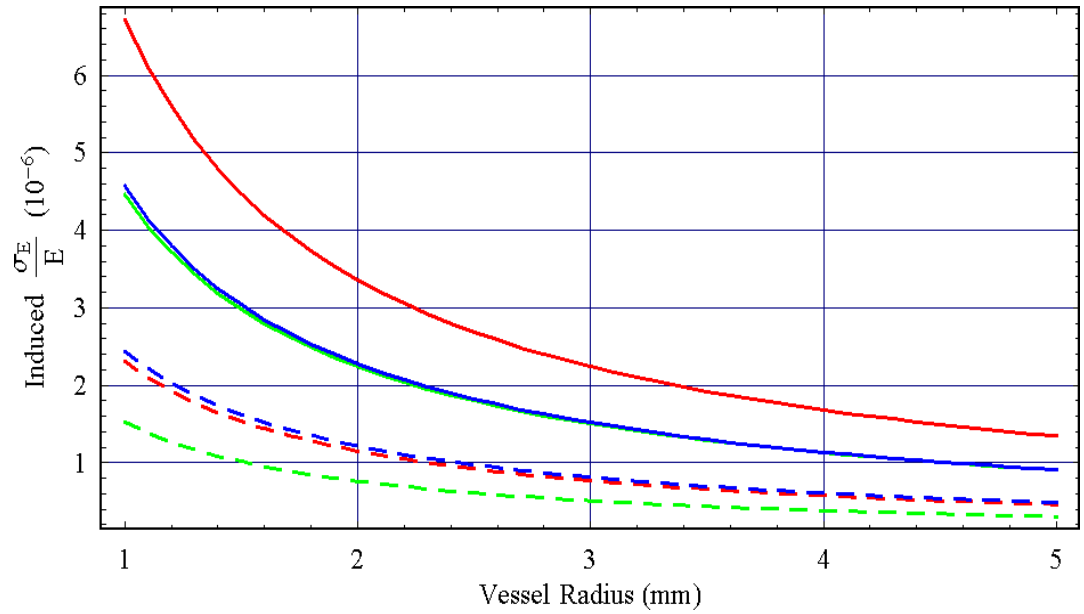

Figure 12: induced energy spread for 200m of undulator for DC (red) AC (blue) and ASE (green) wakes as a function of vessel radius for copper at 273K (solid) and 77K (dashed) for a 500 micron Gaussian bunch.

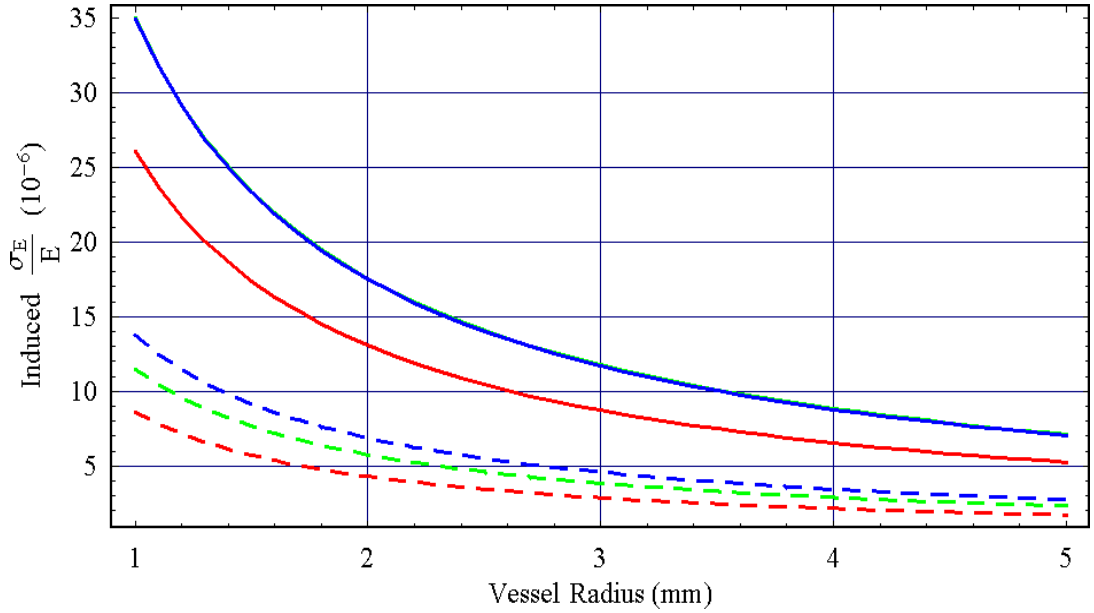

Figure 13 induced energy spread for 200m of undulator for DC (red) AC (blue) and ASE (green) wakes as a function of vessel radius for aluminium at 273K (solid) and 77K (dashed) for a 150 micron Gaussian bunch.

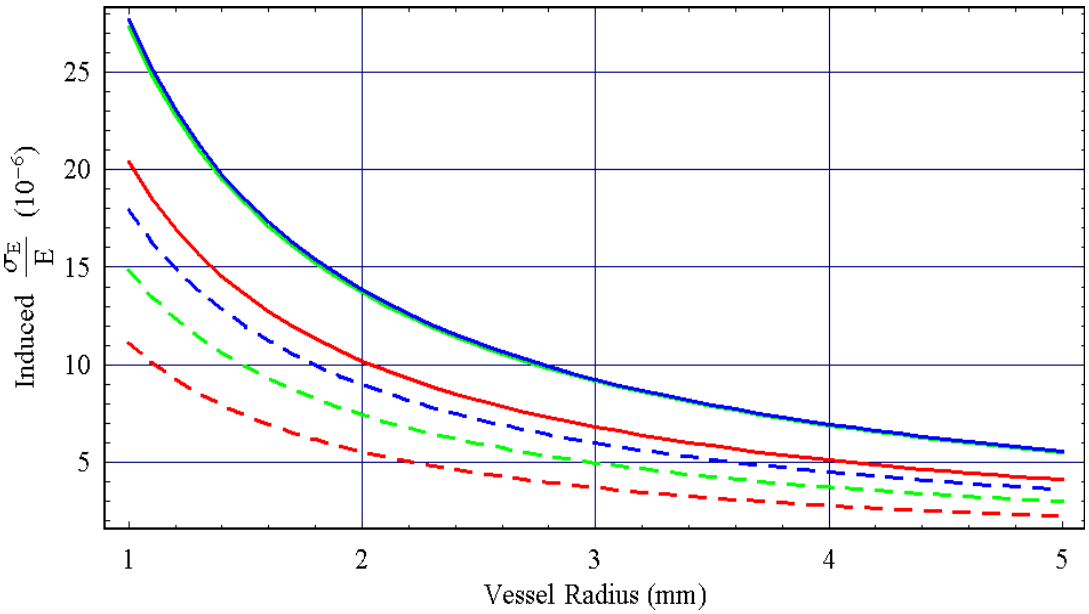

Figure 14: induced energy spread for 200m of undulator for DC (red) AC (blue) and ASE (green) wakes as a function of vessel radius for gold at 273K (solid) and 77K (dashed) for a 150 micron Gaussian bunch.

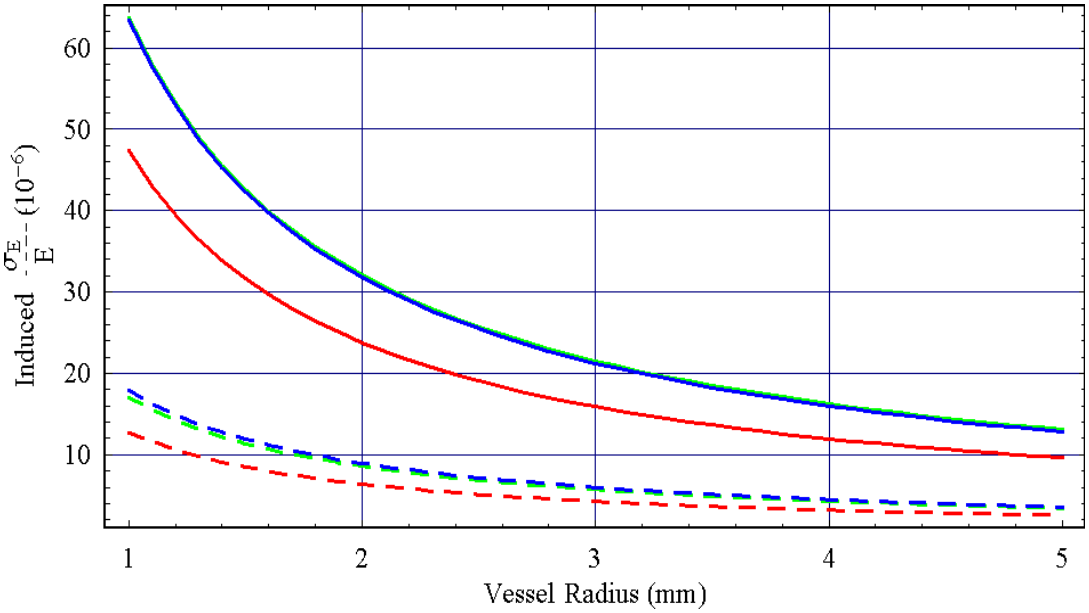

Figure 15: induced energy spread for 200m of undulator for DC (red) AC (blue) and ASE (green) wakes as a function of vessel radius for iron at 273K (solid) and 77K (dashed) for a 150 micron Gaussian bunch.

7. Non Gaussian Bunch Distributions

The wakefield effects could be quite different for non-Gaussian charge distributions. Two different charge distributions have been considered, a trapezium shaped distribution and also one similar to the Linac Coherent Light Source (LCLS) [9], (see Figure 16). These non-Gaussian distributions could have higher frequency components that increase the induced energy spread. RMS bunch lengths of 150, 300

and 500 micron were modelled but only the 150 micron results are presented as they induced the largest energy spread. To give confidence in the results for different charge distributions the numerical techniques were benchmarked against work done on the LCLS undulator vessel [5]. Graphs of the wake potentials for a 2mm copper vessel at 273K and 77K and the induced energy spread as a function of radius are shown in Figure 17 to Figure 23for the two new charge distributions. As with Gaussian bunches the AC and ASE wakes are very similar at 273K and deviate from one another at 77K. There is more ringing in the LCLS bunch but the amplitude is similar so the induced energy spread is not so different as the temperature changes, (Figure 23).

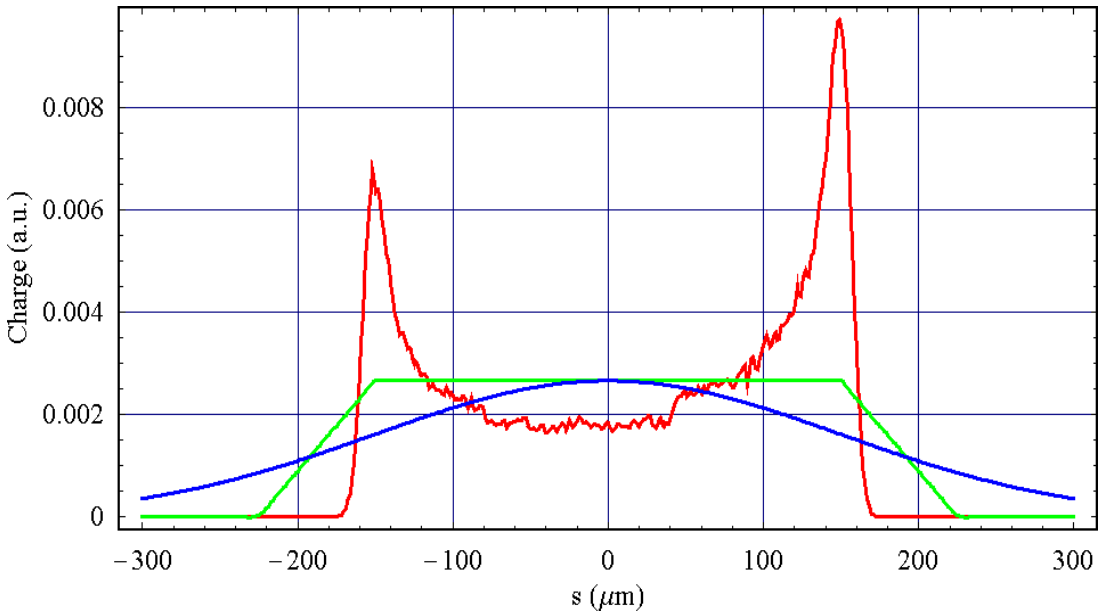

Figure 16: Gaussian (blue), LCLS type (red), and trapezium (green) charge distributions.

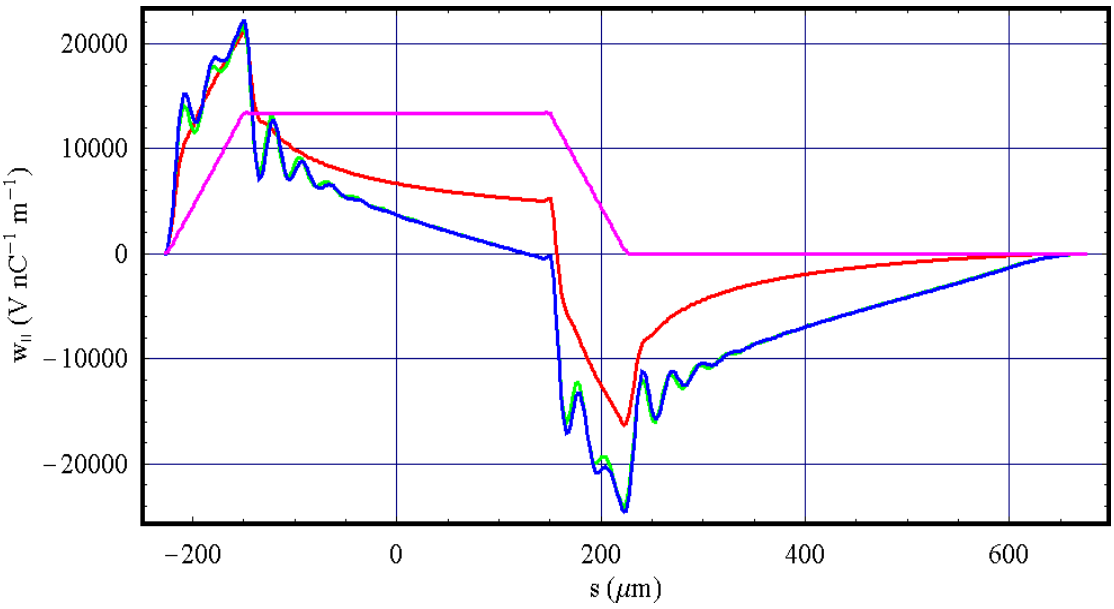

Figure 17: DC (red), AC (green & points) and ASE (blue) wake potentials for a 150 micron trapezium charge distribution (magenta) and a 2mm copper vessel at 273K.

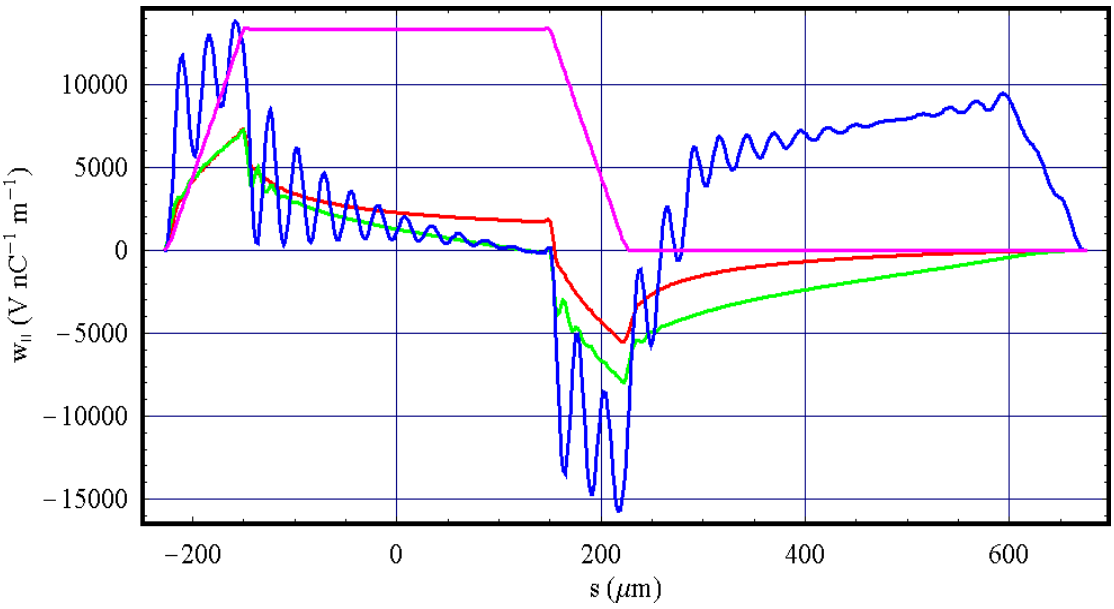

Figure 18: DC (red), AC (green & points) and ASE (blue) wake potentials for a 150 micron trapezium charge distribution (magenta) and a 2mm copper vessel at 77K.

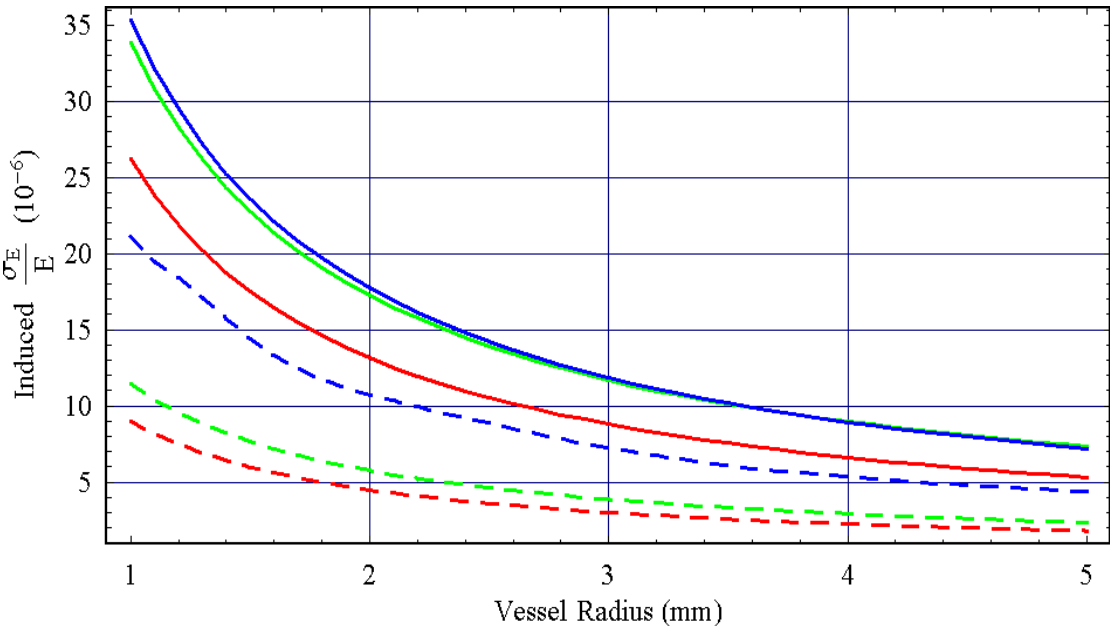

Figure 19: induced energy spread for 200m of undulator for DC (red) AC (blue) and ASE (green) wakes as a function of vessel radius for gold at 273K (solid) and 77K (dashed) for a 150 micron trapezium bunch.

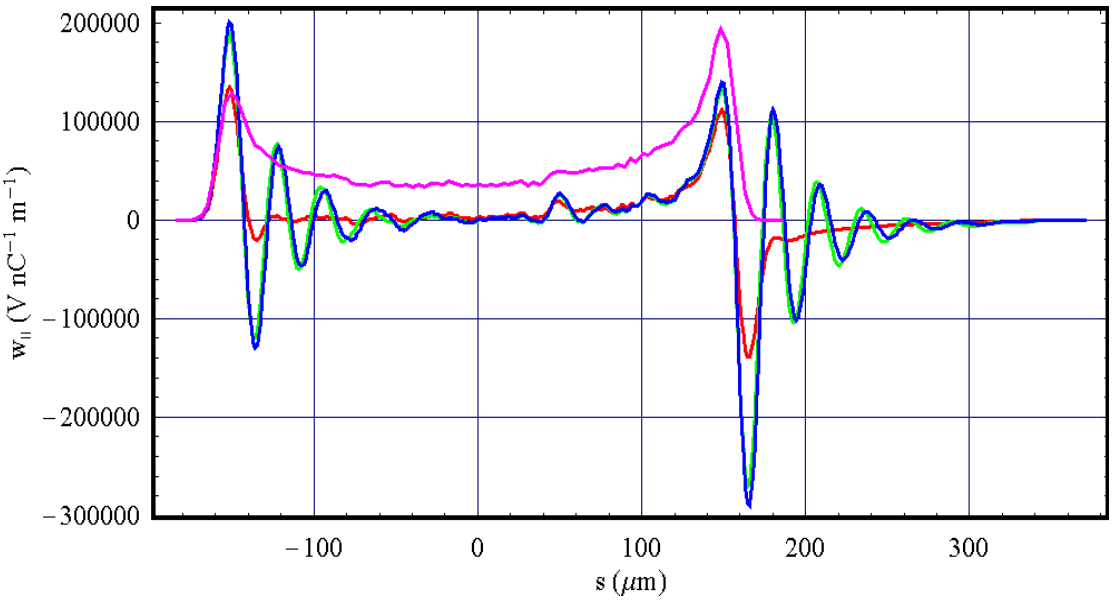

Figure 20: DC (red), AC (green & points) and ASE (blue) wake potentials for a 150 micron LCLS shape charge distribution (magenta) and a 2mm copper vessel at 273K.

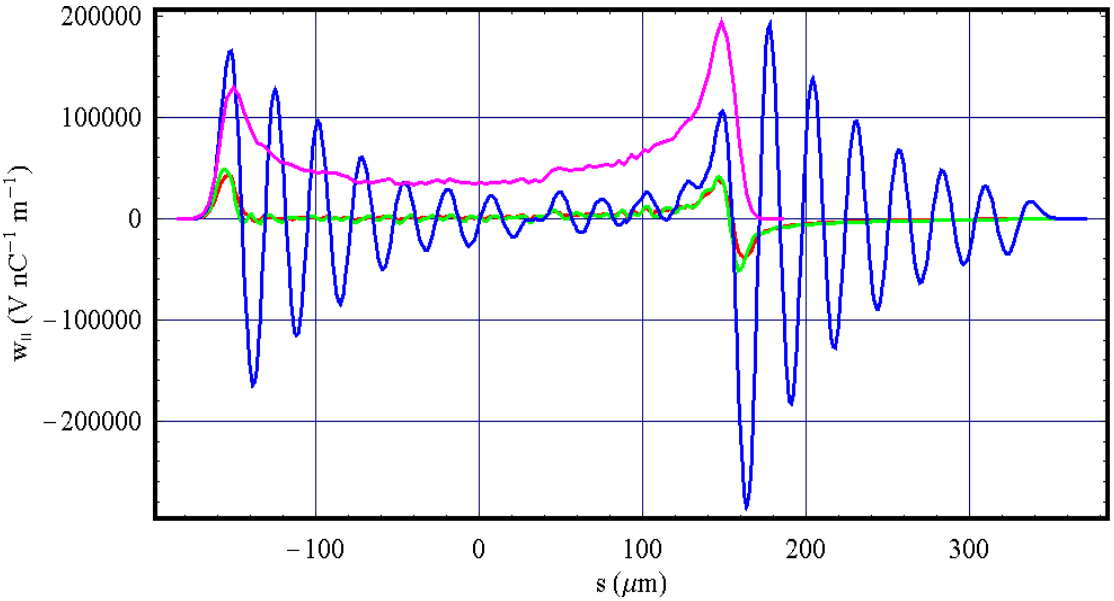

Figure 21: DC (red), AC (green & points) and ASE (blue) wake potentials for a 150 micron LCLS shape charge distribution (magenta) and a 2mm copper vessel at 77K.

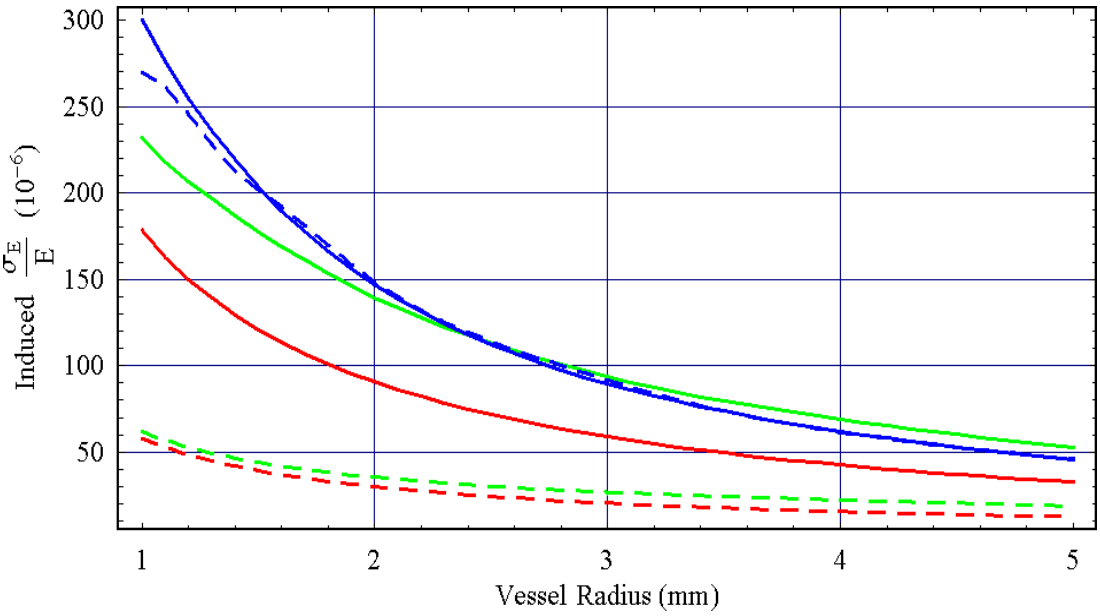

Figure 22: induced energy spread for 200m of undulator for DC (red) AC (blue) and ASE (green) wakes as a function of vessel radius for gold at 273K (solid) and 77K (dashed) for a 150 micron LCLS type bunch.

8. Estimation of the Effects for a Stainless Steel Vessel

The effects of a stainless steel vessel are difficult to asses because the electrical properties greatly depend upon the level of impurities of the metal. The conductivity is relatively simple to measure but a value for the mean time between collisions is also needed. Due to surface roughness effects the main vessel will probably be made from an extremely smooth type 316L stainless steel vessel [10]. The DC conductivity and the mean time between collisions are related by density of conduction electrons in the metal, n:

$$\sigma_{DC} = \frac{ne^2\tau}{m_e}.$$

The density of conduction electrons can be calculated from the mass density ρ_m, atomic weight, A, and number of valence electrons of the material:

$$n = \frac{N_A Z \rho_m}{A},$$

where N_A is Avogadro's number. The radius of a sphere whose volume is equal to the volume per conduction electron, r_s is then:

$$r_s = \left(\frac{3}{4\pi n}\right)^{\frac{1}{3}}.$$

This gives a convenient expression for the relaxation time in seconds [4]:

$$\tau = \left(\frac{0.22}{\rho_\mu} \right) \left(\frac{r_s}{a_0} \right)^3 10^{-14},$$

where ρ_μ is the resistivity in micro-ohm cm and a_0 is the Bohr radius of the atom. As an example copper has a single valence electron, a density of 8.23 g cm^{-3} and an atomic weight of 63.546. This gives an electron density of 7.8 10^{22} g cm^{-3} and a relaxation time of 2.92 10^{-14} s, an often quoted value is 2.7 10^{-14} s [4].

316L Stainless Steel has density of 8 g cm^{-3}, a resistivity of 74.5 micro-ohm cm at room temperature and a number of valence electrons that is not well defined, but four shall be assumed. These numbers give a relaxation time of 1.38 10^{-16} s. This is much shorter than the other pure elements, as expected due to the high levels of impurities that scatter the conduction electrons. The small relaxation time will mean that the AC wakefield will be more important, even at room temperature.

From the wake potentials the induced energy spread can also be calculated, this is shown on a log scale in Figure 23. As can be seen the induced energy spread for the AC wake is not a straight line for the LCLS and trapezium shape bunches as the vessel radius increases. The wavelength for the wake potentials of these two charge distributions changes as the vessel radius is increased, this is not the case for the Gaussian charge distribution, as can be seen in Figure 24, Figure 25 and Figure 26. The trapezium and LCLS charge distributions also have higher frequency components than a Gaussian distribution and so their wakes ring more over the length of the charge distribution. In the convolution of the wake functions with the charge distribution only the Gaussian distribution has a non zero value for all s, which may account for some of this non-linearity.

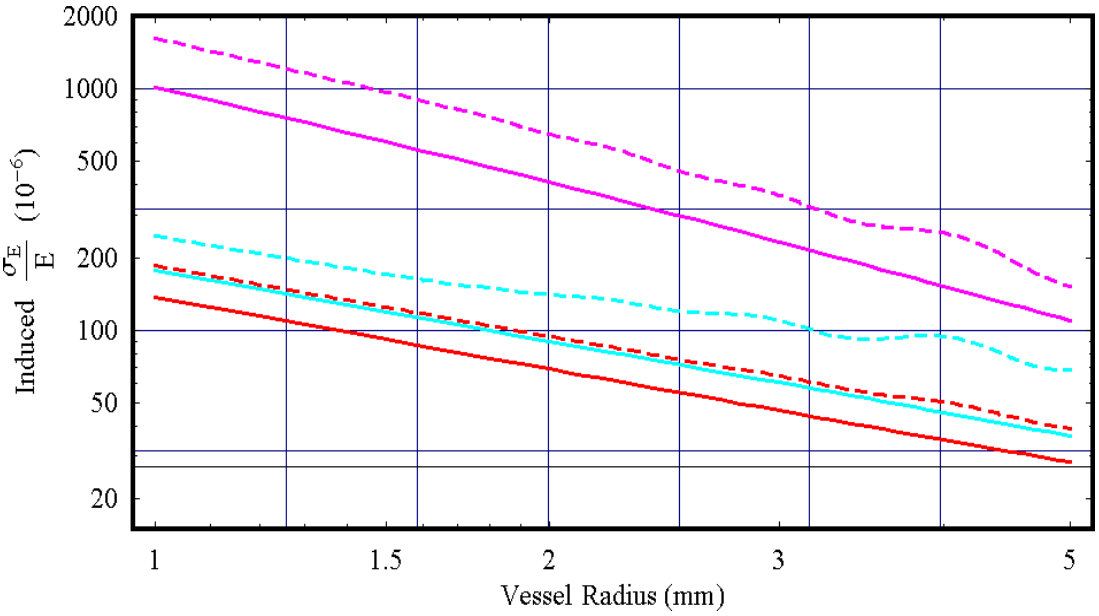

Figure 23: induced energy spread for 200m of undulator for DC (solid) and AC (dashed) wakes as a function of vessel radius for stainless steel with for a 150 micron Gaussian (red), trapezium (cyan) and LCLS (magenta) type charge distributions.

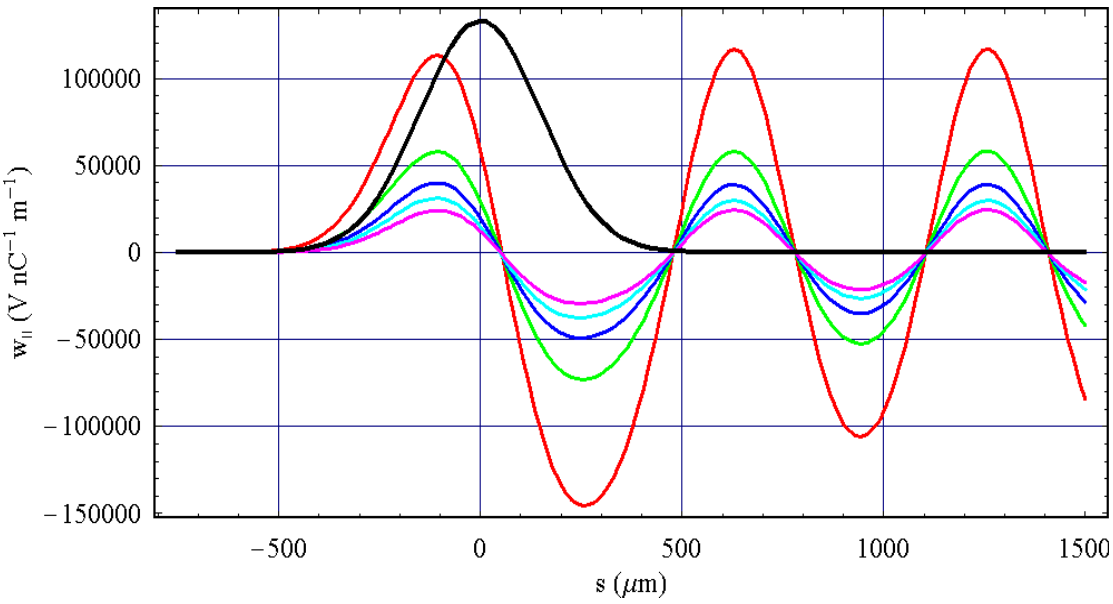

Figure 24: wake potential of a Gaussian charge distribution (black) for 1mm (red), 2mm (green), 3mm (blue), 4mm (cyan) and 5mm (magenta) radius stainless steel vessels.

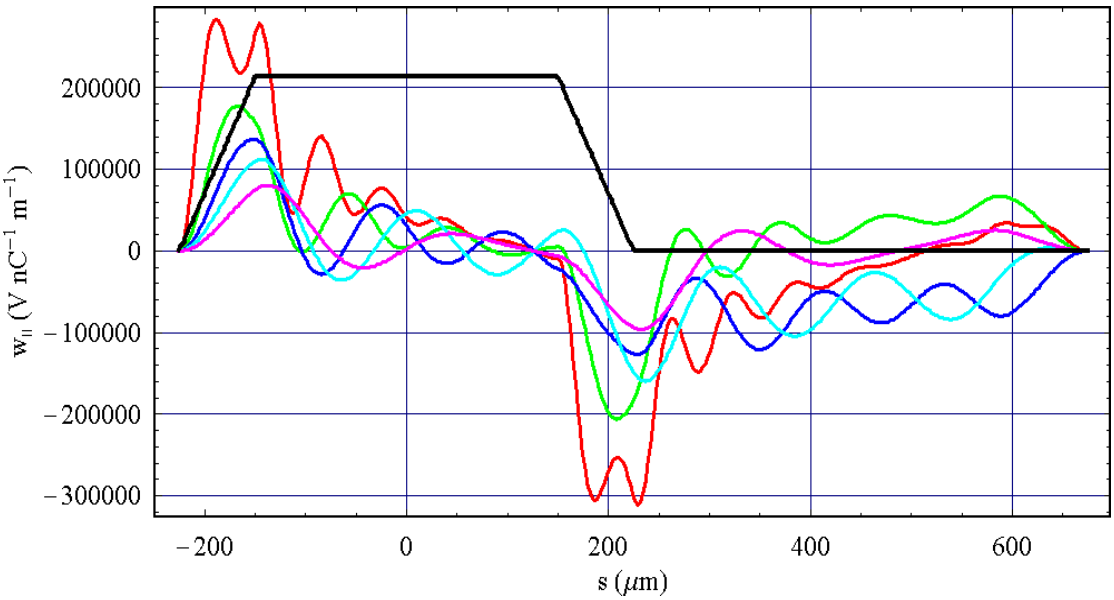

Figure 25: wake potential of a trapezium charge distribution (black) for 1mm (red), 2mm (green), 3mm (blue), 4mm (cyan) and 5mm (magenta) radius stainless steel vessels.

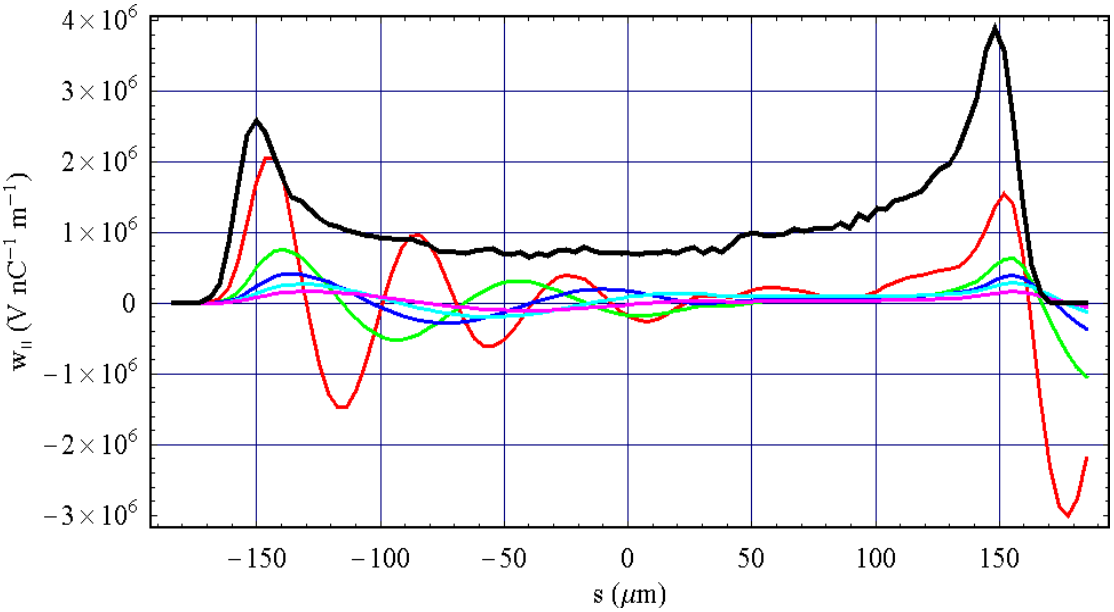

Figure 26: wake potential of a LCLS type charge distribution (black) for 1mm (red), 2mm (green), 3mm (blue), 4mm (cyan) and 5mm (magenta) radius stainless steel vessels.

9. Conclusions & Further Work

The resistive wall wakefields for a round pipe have been calculated. The wakes from copper, gold, aluminium and iron vessel have been calculated at 273K and 77K. An estimation of stainless steel type 316L has been made, it is assumed that because the conduction electron scattering is mainly due to impurities in this material there will not be a strong temperature dependence of the wakefield effects. Three different charge distributions have also been considered as well as the minimum, nominal and maximum ILC parameters set. In all cases the wakes are worst for the

minimum parameter set and at 273K. These have all been calculated as a function of the vessel radius, generally speaking the wakes scale as an inverse power of the radius. Although a 2mm radius vessel has been used as the minimum possible radius currently a vessel ~5.6mm in diameter is being used in the design, so this value should be used to estimate the increase in energy spread. The maximum increase in the energy spread as a percentage of the nominal is shown for the different vessel materials at 273K and 77K for each different charge distribution in Figure 27, Figure 28 and Figure 29.

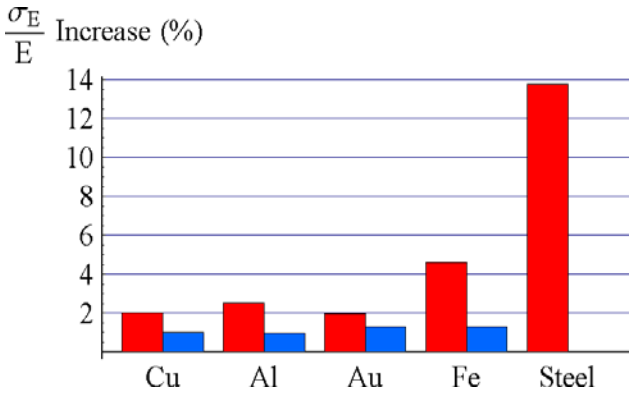

Figure 27: maximum increase in energy spread for a 150 micron Gaussian charge distribution and 200m of undulator with an aperture of 5.6mm for different materials at 273K (red) and 77K (blue).

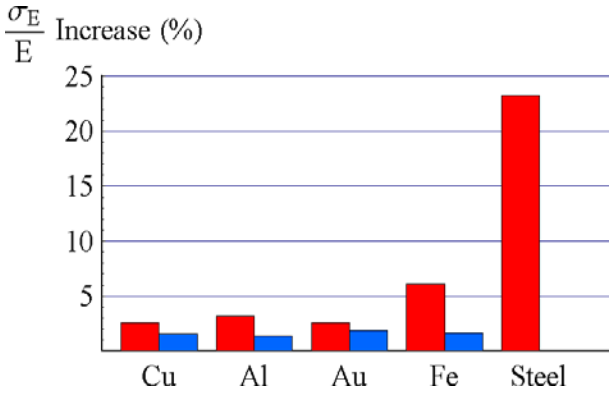

Figure 28: Increase in energy spread for a 150 micron trapezium charge distribution and 200m of undulator with an aperture of 5.6mm for different materials at 273K (red) and 77K (blue).

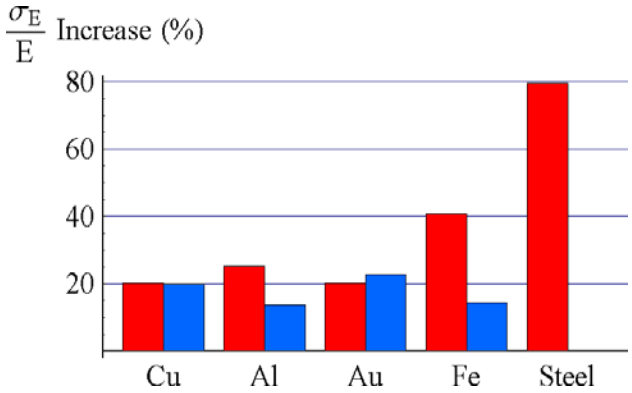

Figure 29: Increase in energy spread for a 150 micron LCLS charge distribution and 200m of undulator with an aperture of 5.6mm for different materials at 273K (red) and 77K (blue).

As can be seen from the charts the estimation of the effects of a steel vessel indicate that it should not be used, if the percentage increase in the energy spread is to be kept below 10%. At 77K aluminium is the best material to use from an increase in energy spread point of view. However, another requirement is that the rms surface roughness of the vessel should be below ~300nm [10]. Initially only a stainless steel vessel could be found that met the roughness requirement however now a copper pipe has been found with an Ra surface roughness of ~100nm [11]. The results for stainless steel indicate that a vessel made of this material would have to be coated with copper or gold to minimise the induced energy spread. Coating such a narrow gap vessel with a smooth layer of copper or gold would not be easy. For this reason a smooth copper pipe will be used as the vacuum vessel.

The results for an LCLS type charge distribution show the most dramatic increase in energy spread, this is due to the high frequency components. The ILC charge distribution through the undulator is expected to be a Gaussian, or close to a Gaussian, and so the 20% increase in energy spread from an LCLS type distribution is not considered to be a realistic possibility for the ILC. When a more realistic charge distribution is known for the beam at the undulator then this can be checked.

The temperature dependence of the wakefields for Gaussian and trapezium shaped bunches show that as the temperature decreases so does the induced energy spread. Although reliable numbers are not available for materials at 4K, the operating temperature of the vessel, it is likely that the effects will continue to improve, or get no worse, as the temperature decreases. Therefore an increase of 1.3% for copper/gold at 77K can be thought of as a worst case scenario.

10. References

1 D.J. Scott "*An Introduction to Resistive Wall Wakefields And Initial Calculations of Their Effects for the Helical Undulator for TESLA*" ASTEC-ID-032
2 A. Chao "*The Physics of Collective Beam Instabilities in High Energy Accelerators,*" John Wiley & Sons, 1993
3 Palumbo *et al* "*Wake Fields and Impedance*" CAS-95-06 Volume 1
4 Ashcroft & Mermin "*Solid State Physics*" Holt, Rinehart & Winston, 1976
5 K.L.F.Bane '*Resistive Wall Wakefield in the LCLS Undulator Beam Pipe*' SLAC-PUB-10707, Revised October 2004
6 J.D. Jackson "*Classical Electro-Dynamics,"* John Wiley & Sons, 1975
7 G.E.H Reuter & E.H. Sondheimer "*The Theory of the Anomalous Skin Effect in Metals*" Proc. Roy. Soc.Lond A195, Pg336, 1949
8 K.L.F. Bane '*The Short Range Resistive Wall Wakefields*' SLAC/AP-87 June 1991
9 Provided by P.Emma, private communication.
[10] D.J. Scott "Surface Roughness Wakefields for the ILC Positron Undulator Vessel" ASTEC-ID-039/Cockcroft-06-10
[11] Provided by Swagelok, see, http://www.swagelok.com/